Molecular Biology of the Cell
Vol. 17, 2465–2475, May 2006

JRAB/MICAL-L2 Is a Junctional Rab13-binding Protein Mediating the Endocytic Recycling of Occludin

Tomoya Terai,*† Noriyuki Nishimura,* Ikuno Kanda,* Natsuo Yasui,† and Takuya Sasaki*

*Departments of Biochemistry and †Orthopedics, Institute of Health Biosciences, University of Tokushima Graduate School, Tokushima 770-8503, Japan

Submitted September 2, 2005; Revised February 21, 2006; Accepted February 27, 2006
Monitoring Editor: Asma Nusrat

The dynamic turnover of tight junctions (TJs) is essential for epithelial–mesenchymal transitions and/or mesenchymal–epithelial transitions during epithelial morphogenesis. We previously demonstrated that Rab13 specifically mediates the endocytic recycling of occludin. Here, we identified MICAL-L2 (molecule interacting with CasL-like 2) as a novel Rab13-binding protein. Immunoprecipitation and immunofluorescence microscopy showed that MICAL-L2 specifically bound to the GTP-bound form of Rab13 via its C terminus, which contained a coiled-coil domain, and localized at TJs in epithelial MTD-1A cells. Recycling assay demonstrated that a MICAL-L2 mutant lacking the Rab13-binding domain (MICAL-L2-N) specifically inhibited the endocytic recycling of occludin but not transferrin receptor. Ca^{2+} switch assay further revealed that MICAL-L2-N as well as Rab13 Q67L inhibited the recruitment of occludin to the plasma membrane, the development of transepithelial electrical resistance, and the formation of a paracellular diffusion barrier. MICAL-L2 was displaced from TJs upon actin depolymerization and was distributed along radiating actin cables and stress fibers in Ca^{2+}-depleted MTD-1A and fibroblastic NIH3T3 cells, respectively. These results suggest that MICAL-L2 mediates the endocytic recycling of occludin and the formation of functional TJs by linking Rab13 to actin cytoskeleton. We rename MICAL-L2 as JRAB (*j*unctional *Rab*13-binding protein).

INTRODUCTION

Rab family small G proteins are key regulators of membrane traffic (Takai *et al*., 2001; Zerial and McBride, 2001; Pfeffer and Aivazian, 2004; Seabra and Wasmeier, 2004). In mammalian cells, there are at least 63 different Rab family members, which recognize distinct subsets of intracellular membranes. Rab proteins act as molecular switches, cycling between "inactive" GDP-bound and "active" GTP-bound forms. This cyclical activation and inactivation are tightly coupled to its membrane association/dissociation cycle; to be in a fully active state, Rab proteins must be both GTP bound and membrane associated. These events are coordinated by several factors. Inactive GDP-bound Rab proteins form stable complexes with GDP dissociation inhibitor (GDI) in the cytosol. Rab–GDI complexes are delivered to their target membranes, where Rab proteins are dissociated from GDI by GDI displacement factor and then activated by GDP/GTP exchange protein (GEP). Active GTP-bound Rab proteins interact with their specific effector protein(s), which mediate a variety of Rab activities. GTP hydrolysis catalyzed by GTPase-activating protein returns Rab proteins to their inactive GDP-bound form. Inactive GDP-bound Rab proteins are extracted from the membranes by GDI and returned to the cytosol. This cyclical activation coupled with membrane association allows both spatial and temporal control of Rab activity. In vesicular transport, Rab proteins regulate vesicle budding, cytoskeleton-dependent motility, and membrane tethering and fusion. Rab proteins are also implicated in controlling cytoskeleton-dependent motility of organelles, in organizing functionally distinct membrane domains within a particular organelle, and in defining organella identity. Now increasing evidence indicate a role of Rab proteins in coordinating membrane tethering and fusion with cytoskeleton (Jordens *et al*., 2005).

Tight junctions (TJs) are continuous, circumferential belt-like structures located at the apical end of the intercellular space, where they delineate the boundaries between the apical and basolateral domains of the plasma membrane (PM) of epithelial cells, and regulate the passage of water, ion, and solutes through the paracellular pathway (Tsukita *et al*., 2001; Anderson *et al*., 2004; Schneeberger and Lynch, 2004). It is clear that TJs are not absolute and static barriers but are instead very plastic cellular structures that are subjected to dynamic remodeling during epithelial–mesenchymal transitions (EMT) and/or mesenchymal-epithelial transitions (MET) (Schock and Perrimon, 2002; Thiery, 2003). TJs are composed of integral TJ proteins and TJ plaque proteins. Integral TJ proteins, including occludin and claudins, mediate cell–cell adhesion and create physical intercellular barrier (Furuse *et al*., 1993; Furuse *et al*., 1998a). Although the precise function of occludin has not yet been established, claudins, which comprise a multigene family consisting of at least 24 members in mammals, are now thought to be an indispensable structural component of TJ strands (Furuse *et*

This article was published online ahead of print in *MBC in Press* (http://www.molbiolcell.org/cgi/doi/10.1091/mbc.E05–09–0826) on March 8, 2006.

Address correspondence to: Takuya Sasaki (sasaki@basic.med.tokushima-u.ac.jp).

Abbreviations used: CC, coiled-coil; EMT, epithelial–mesenchymal transition; MET, mesenchymal-epithelial transition; PM, plasma membrane; TER, transepithelial electrical resistance; TfR, transferrin receptor; TJ, tight junction; ZO, zonula occludens.

al., 1998b; Saitou *et al*., 1998; Saitou *et al*., 2000). TJ plaque proteins clustered integral TJ proteins and formed an organizing platform for a variety of scaffolding, signaling, and vesicular transport proteins. In addition to specific TJ proteins, a circumferential actin belt that encircled each epithelial cell at the level of TJs was critical for formation and maintenance of TJs (Vasioukhin and Fuchs, 2001; Bershadsky, 2004). Among an increasing number of TJ plaque proteins, zonula occludens (ZO) family proteins, cingulin, and junction-associated coiled-coil protein (JACOP) were shown to bind to F-actin and implicated in linking TJs to a circumferential actin belt (Wittchen *et al*., 1999; D'Atri and Citi, 2001; Ohnishi *et al*., 2004). However, the molecular mechanisms governing the dynamic turnover of TJs remain elusive.

Two Rab family members, Rab3B and Rab13, were identified as TJ plaque proteins in epithelial cells (Weber *et al*., 1994; Zahraoui *et al*., 1994). Rab13 was expressed in both fibroblastic and epithelial cells and was implicated in the assembly of functional TJs and neuronal plasticity (Zahraoui *et al*., 1994; Marzesco *et al*., 2002; Di Giovanni *et al*., 2005). Recently, it was suggested that the GTP-bound form of Rab13 bound to protein kinase A (PKA) and negatively controlled the PKA-dependent phosphorylation and recruitment of vasodilator-stimulated phosphoprotein to the TJs (Lawrence *et al*., 2002; Kohler *et al*., 2004). We previously found that occludin was subject to the endocytic recycling, and identified Rab13 as its crucial regulator (Morimoto *et al*., 2005). In the present study, we have identified MICAL-L2 (molecule interacting with CasL-like 2) as a novel Rab13-binding protein using yeast two-hybrid screening. MICAL-L2 was expressed in both fibroblastic and epithelial cells and was localized to TJs in epithelial cells. We found that MICAL-L2 as well as Rab13 mediated the endocytic recycling of occludin, but not transferrin receptor (TfR), and the formation of functional TJs. We rename MICAL-L2 as *j*unctional *Rab*13-binding protein (JRAB).

MATERIALS AND METHODS

Plasmid Construction

A full-length cDNA of JRAB/MICAL-L2 (GenBank/EMBL/DDBJ accession no. AB182579) was obtained by reverse transcription (RT)-PCR from mouse brain cDNA. JRAB-F (amino acids 1-1009), JRAB-N (amino acids 1-805), and JRAB-C (amino acids 806-1009) cDNAs were generated by PCR using full-length JRAB cDNA as a template. The mammalian expression vector pCI-neo-Myc was used to express N-terminal Myc-tagged JRAB-F, JRAB-N, and JRAB-C proteins. Rab1A, Rab5A, and Rab13 cDNAs were isolated by RT-PCR from Madin-Darby canine kidney (MDCK), MDCK, and Caco2 cells, respectively. Rab13 T22N, Rab13 Q67L, and Rab13 N121I mutants were constructed using the QuikChange mutagenesis kit (Stratagene, La Jolla, CA). The mammalian expression vector pCI-neo-HA was used to express N-terminal hemagglutinin (HA)-tagged Rab1A, Rab5A, Rab13, Rab13 T22N, Rab13 Q67L, and Rab13 N121I proteins. All plasmids constructed in this study were sequenced using an ABI Prism 3100 genetic analyzer (Applied Biosystems, Foster City, CA).

Two-Hybrid Screening

Rab1A, Rab5A, Rab13, Rab13 T22N, Rab13 Q67L, and Rab13 N121I were cloned into the yeast two-hybrid bait vector pGBDU-C1 (James *et al*., 1996). A mouse 11-d-old embryo cDNA library in the yeast two-hybrid prey vector pACT2 was purchased from Clontech (Mountain View, CA). The yeast strain PJ69-4A (*MATa trp1-901 leu2-3112 ura3-52 his3-200 gal4*Δ*gal80*Δ *GAL2-ADE2 LYS2::GAL1-HIS3 met2::GAL7-lacZ*) was sequentially transformed with pGBDU-Rab13 Q67L and the mouse 11-d-old embryo cDNA library. Two-hybrid screening was performed and evaluated as described previously (James *et al*., 1996). Standard procedures for yeast manipulations were as described previously (Kaiser *et al*., 1994).

Antibodies

JRAB-C (amino acids 806-1009) was cloned into pGEX-6P1 vector to express N-terminal glutathione *S*-transferase (GST)-tagged JRAB-C protein. GST and GST-JRAB-C fusion proteins were produced in *Escherichia coli* strain DH5α and purified using glutathione-Sepharose beads (GE Healthcare, Piscataway, NJ) according to the manufacturer's instructions. Two milligrams of GST or GST-JRAB-C protein was immobilized on HiTrap NHS-activated columns (GE Healthcare) according to the manufacturer's instructions. Two female Wistar rats were immunized with 100 μg of GST-JRAB-C protein twice at 4-wk intervals, after which whole blood was collected. Crude immunoglobulin (Ig) fractions were prepared by ammonium sulfate precipitation and passed through a GST-immobilized column to remove an anti-GST antibody. The anti-JRAB polyclonal antibody was further purified on a GST-JRAB-C–immobilized column according to the manufacturer's instructions. The rat anti-occludin (MOC37) antibody was a kind gift from Dr. S. Tsukita (Kyoto University, Kyoto, Japan). Rabbit anti-ZO-1 and mouse anti-TfR antibodies were purchased from Zymed Laboratories (South San Francisco, CA), mouse anti-Myc (9E10) was from American Type Culture Collection (Manassas, VA), mouse anti-HA (12CA5) and rat anti-HA (3F10) were from Roche Diagnostics (Mannheim, Germany), and rabbit anti-green fluorescent protein (GFP) was from Invitrogen (Carlsbad, CA).

Cell Culture and Transfection

MTD-1A and L cells were kindly supplied by Dr. S. Tsukita. Baby hamster kidney (BHK), MDCK, NIH3T3, and Caco2 cells were obtained from American Type Culture Collection. BHK, MTD-1A, and NIH3T3 cells were cultured at 37°C (5% CO_2 and 95% air) in DMEM with 10% fetal bovine serum (FBS). BHK and MTD-1A cells were transfected using Lipofectamine 2000 transfection reagent (Invitrogen) according to the manufacturer's instructions.

Coimmunoprecipitation

Thirty-six hours after transfection, BHK and MTD-1A cells were lysed with 25 mM Tris-HCl, pH 7.5, containing 0.5% 3-[(3-cholamidopropyl)dimethylammonio]propanesulfonate (CHAPS), 125 mM NaCl, 1 mM $MgCl_2$, 10 μg/ml (4-amidinophenyl)-methanesulfonyl fluoride (APMSF), and 100 μM guanosine 5′-*O*-(3-thio)triphosphate (GTPγS)/GDP for 15 min at 4°C. After removing a fraction of the lysates, the remaining lysates were immunoprecipitated with anti-HA (12CA5) antibody bound to protein G-Sepharose beads (GE Healthcare) and washed three times with 25 mM Tris-HCl, pH 7.5, containing 0.1% CHAPS, 300 mM NaCl, 1 mM $MgCl_2$, and 10 μM GTPγS/GDP. The samples were prepared for Western blot analysis.

Subcellular Fractionation

MTD-1A cells were homogenized in 20 mM Tris-HCl, pH 7.5, containing 100 mM NaCl, 1 mM $MgCl_2$, and 10 μg/ml APMSF using a ball bearing homogenizer (HGM Precision Engineering, Heidelberg, Germany). The lysates were first centrifuged at 800 × *g* for 10 min at 4°C, and the resulting postnuclear supernatant (PNS) fractions were taken. The PNS fractions were further centrifuged at 100,000 × *g* for 60 min at 4°C in a Hitachi S100AT2 rotor (Hitachi, Tokyo, Japan) to obtain S100 and P100 fractions. PNS, S100, and P100 fractions were subjected to Western blot analysis.

Western Blot

Each sample was separated by SDS-PAGE, and proteins were transferred to a polyvinylidene diflouride (PVDF) membrane. Membrane blocking and antibody dilutions were done in Block Ace (Dainippon Pharmaceutical, Osaka, Japan). Blots were developed by chemiluminescence using a horseradish peroxidase-coupled secondary antibody (Jackson ImmunoResearch Laboratories, West Grove, PA) with an ECL-Plus kit (GE Healthcare). Quantitation was performed on scans of autoradiograph films with nonsaturated signals using NIH Image 1.62 software (http://rsb.info.nih.gov/nih-image/).

Immunofluorescence Microscopy

BHK cells were grown on glass coverslips and fixed with 2% formaldehyde in phosphate-buffered saline (PBS) for 15 min at room temperature. MTD-1A and NIH3T3 cells, grown on Transwell filters (Corning, Acton, MA) or glass coverslips, were fixed with 10% trichloroacetic acid in PBS for 15 min on ice or 1% formaldehyde in PBS for 15 min at room temperature. After permeabilization with 0.2% Triton X-100 in PBS for 15 min and blocking with 5% goat serum in PBS for 60 min at room temperature, cells were incubated with primary antibodies for 60 min and with Alexa 488- or Alexa 594-conjugated secondary antibodies (Invitrogen) for 60 min at room temperature. F-actin was labeled with rhodamine-phalloidin (Invitrogen). Fluorescent images were acquired using a Radiance 2000 confocal laser scanning microscope (Bio-Rad, Hercules, CA).

Recombinant Adenovirus Infection

Recombinant adenovirus expressing EGFP and EGFP-Rab13 Q67L (Ad-EGFP and Ad-EGFP-Rab13 Q67L) were described previously (Morimoto *et al*., 2005). Recombinant adenovirus expressing Myc-JRAB-F (Ad-Myc-JRAB-F), Myc-JRAB-N (Ad-Myc-JRAB-N), and Myc-JRAB-C (Ad-Myc-JRAB-C) were constructed using the Transpose-Ad Adenoviral Vector System (Qbiogene, Carlsbad, CA). Briefly, Myc-JRAB-F, Myc-JRAB-N, and Myc-JRAB-C cDNAs were cloned into a pCR259 transfer vector. Then, a recombinant adenoviral plasmid was generated by Tn7-mediated transposition in *E. coli*. The resulting

plasmid was linearized by PacI-digestion and transfected into QBI-HEK293 cells using the MBS Mammalian Transfection kit (Stratagene, La Jolla, CA). After 24 h, the cells were split into a 96-well plate and incubated at 37°C for 10–14 d. Screening of recombinant adenovirus was performed by PCR and Western blot analysis. Recombinant adenovirus was amplified in QBI-HEK293 cells and its titer was determined by MOI test. MTD-1A cells were infected with Ad-EGFP, Ad-Myc-JRAB-N, and Ad-EGFP-Rab13 Q67L at a MOI of 100. Twenty-four h later, the cells were subjected to an endocytosis or recycling assay.

Endocytosis and Recycling Assays

Endocytosis and recycling assays was performed as described previously (Le *et al*., 1999; Morimoto *et al*., 2005). Briefly, cell surface proteins were biotinylated with 0.5 mg/ml Sulfo-NHS-SS-Biotin (Pierce Chemical, Rockford, IL) in PBS containing 0.9 mM $CaCl_2$ and 0.33 mM $MgCl_2$ (PBS/CM) at 4°C for 30 min, quenched with 50 mM NH_4Cl in PBS/CM at 4°C for 15 min, and incubated at 37°C for the indicated periods to allow endocytosis. The remaining biotin on the cell surface was stripped with 50 mM 2-mercaptoethanesulfonic acid (MESNA) in 100 mM Tris-HCl, pH 8.6, containing 100 mM NaCl and 2.5 mM $CaCl_2$ at 4°C for 30 min, and quenched with 5 mg/ml iodoacetoamide in PBS/CM at 4°C for 15 min. In endocytosis assay, cells were then subjected to lysis, isolation of biotinylated cargo proteins, and Western blot analysis.

In recycling assay, cells were again incubated at 37°C for the indicated periods to allow recycling of endocytosed cargo proteins back to the cell surface. Subsequently, the newly appearing cell surface biotin was again stripped with 50 mM MESNA in 100 mM Tris-HCl, pH 8.6, containing 100 mM NaCl and 2.5 mM $CaCl_2$ at 4°C for 30 min and quenched with 5 mg/ml iodoacetoamide in PBS/CM at 4°C for 15 min. After lysis with 50 mM Tris-HCl, pH 8.0, containing 1.25% Triton X-100, 0.25% SDS, 150 mM NaCl, 5 mM EDTA, and 10 μg/ml APMSF, an aliquot was taken to determine the total amount of cargo proteins expressed in the cells. Biotinylated cargo proteins were then isolated with UltraLink-immobilized Neutravidin Plus beads (Pierce Chemical). The samples were prepared for Western blot analysis. The values for biotinylated cargo proteins protected from MESNA treatment were normalized to total cargo proteins expressed in the cells.

Ca^{2+} Switch Assay

Ca^{2+} switch assay was performed as described previously (Kartenbeck *et al*., 1991). Briefly, MTD-1A cells were grown in DMEM with 10% FBS (normal Ca^{2+} ion medium, NCM) and sequentially incubated in Ca^{2+}-free minimal essential medium without FBS (low Ca^{2+} ion medium, LCM) for 1 h and in LCM with 20 mM EGTA for 2 h to remove extracellular Ca^{2+}. Cells were then incubated in NCM for 0, 4, 6, and 24 h and processed for immunofluorescence microscopy.

Measurement of Transepithelial Electrical Resistance (TER)

MTD-1A cells were plated onto Transwell filters (polycarbonate membranes with 12-mm-diameter and 0.4-μm pore size; Corning) as an instant confluent monolayer and grown in NCM for 72–96 h. Cells were then infected with adenoviral-enhanced green fluorescent protein (Ad-EGFP), Ad-Myc-JRAB-N, or Ad-EGFP-Rab13 Q67L for 24 h and subjected to a Ca^{2+} switch assay in which the incubation in LCM with 20 mM EGTA was shortened to 10 min. TER was measured directly in culture media at 0, 12, 24, and 48 h after restoring Ca^{2+} using a Millicell-ERS epithelial voltohmmeter (Millipore, Billerica, MA). TER values were calculated by subtracting the background TER of blank filters and by multiplying the surface area of the filter.

Measurement of Paracellular Tracer Flux

Paracellular tracer flux was measured using 4- and 40-kDa fluorescein isothiocyanate (FITC)-dextran (Sigma-Aldrich, St. Louis, MO). MTD-1A cells were plated onto Transwell filters, infected with Ad-EGFP, Ad-Myc-JRAB-N, or Ad-EGFP-Rab13 Q67L, and subjected to the Ca^{2+} switch assay as described above. Paracellular tracer flux was measured at 12 h after restoring Ca^{2+}. Four- and 40-kDa FITC-dextran was dissolved in P buffer (10 mM HEPES/NaOH, pH 7.4, 1 mM sodium pyruvate, 10 mM glucose, 3 mM $CaCl_2$, and 145 mM NaCl) at a concentration of 20 mg/ml and dialyzed against the same buffer. The apical and basolateral culture media were replaced with P buffer containing 5 mg/ml FITC-dextran and plain P buffer, respectively, and the cells were incubated at 37°C for 5 h. The amount of FITC-dextran diffused from the apical to the basolateral side was measured by a Hitachi F-3010 fluorometer (excitation, 490 nm; emission, 530 nm).

RESULTS

JRAB/MICAL-L2 Is Identified as a Rab13-binding Protein

To gain insight into the molecular mechanisms of Rab13 action, we screened a yeast two-hybrid library constructed from a mouse 11-d-old embryo cDNA using a dominant active mutant of Rab13 (Rab13 Q67L) that is defective in GTP hydrolysis as bait. From 2.4×10^6 clones screened, we obtained three independent clones, which specifically interacted with Rab13 Q67L. These positive clones contained identical sequences and one of these clones, TTY124, was examined in more detail. To examine the guanine nucleotide specificity of the interactions, we generated a dominant negative mutant of Rab13 (Rab13 T22N) that has a lower affinity for GTP than for GDP, and an empty mutant (Rab13 N121I) that is defective in binding to both GDP and GTP. The prey clone specifically bound to wild-type Rab13 (Rab13 WT) and Rab13 Q67L, but not to Rab13 T22N or Rab13 N121I, in the same two-hybrid assay (Figure 1A). The clone also displayed specificity for Rab13, because it was not capable of binding to Rab1A or Rab5A as verified by the same assay (Figure 1A). A sequence database search showed that the clone encodes a 663-base pair sequence of the C-terminal region of AK044547 (GenBank/EMBL/DDBJ). A mouse full-length clone was isolated by RT-PCR from mouse brain cDNA. Sequence analysis of multiple clones revealed a G insertion, A-to-C substitution, and a G-to-A substitution at positions 1613, 1997, and 3031 of AK044547, respectively. The resulting consensus clone encodes a 1009 amino acid protein, which is likely an isoform of mouse MICAL-L2 (GenBank/EMBL/DDBJ accession no. NM174850). MICAL (molecule interacting with CasL), originally identified on the basis of its interaction with CasL, was implicated in Semapholin-Plexin–mediated axonal repulsion (Suzuki *et al*., 2002; Terman *et al*., 2002). Although MICAL-L2 was identified as a MICAL-related cDNA in the GenBank/EMBL/DDBJ Data Bank, no experimental analysis of MICAL-L2 has been reported (Terman *et al*., 2002). Therefore, we rename MICAL-L2 as JRAB (GenBank/EMBL/DDBJ accession no. AB182579). JRAB has a calponin-homology (CH) domain in its N-terminal region (amino acids 3-102), a LIM domain in its middle region (amino acids 187-241), and a coiled-coil (CC) domain at the C terminus (amino acids 842-880) (Figure 1B). All prey clones contained the CC domain but not the LIM and CH domains.

The C-terminal Domain of JRAB Specifically Interacts with GTP-bound Form of Rab13

To confirm the yeast two-hybrid interactions between JRAB and Rab13 in intact cells, we performed coimmunoprecipitation. Myc-tagged full-length JRAB (Myc-JRAB-F; amino acids 1-1009), Myc-tagged N-terminal JRAB (Myc-JRAB-N; amino acids 1-805) containing the LIM and CH domains, or Myc-tagged C-terminal JRAB (Myc-JRAB-C; amino acids 806-1009) containing the CC domain was cotransfected with HA-tagged Rab13 WT (HA-Rab13) into BHK cells. The lysate was first immunoprecipitated with anti-HA antibody bound to protein G-Sepharose beads in the presence of GTPγS to pull down the GTP-bound form of HA-Rab13. Then, the immunoprecipitates were subjected to Western blot analysis using an anti-Myc antibody. HA-Rab13 interacted with Myc-JRAB-F and Myc-JRAB-C, but not with Myc-JRAB-N (Figure 1C, lanes 3–5), indicating that the C terminus of JRAB is responsible for Rab13 binding. We next examined whether JRAB could interact with other Rab family proteins. Myc-JRAB-F interacted with HA-Rab13, but not with HA-Rab1A and HA-Rab5A, by coimmunoprecipitation assay (Figure 1C, lanes 1–3). When the binding of Myc-JRAB-F to HA-Rab13 was analyzed in the presence of either GTPγS or GDP, Myc-JRAB-F preferentially interacted with HA-Rab13 in the presence of GTPγS (Figure 1C, lanes 6 and 7). If JRAB interacts with the GTP-bound form of Rab13 within cells, the two molecules should be colocalized at specific sites. To test this, we have performed double immu-

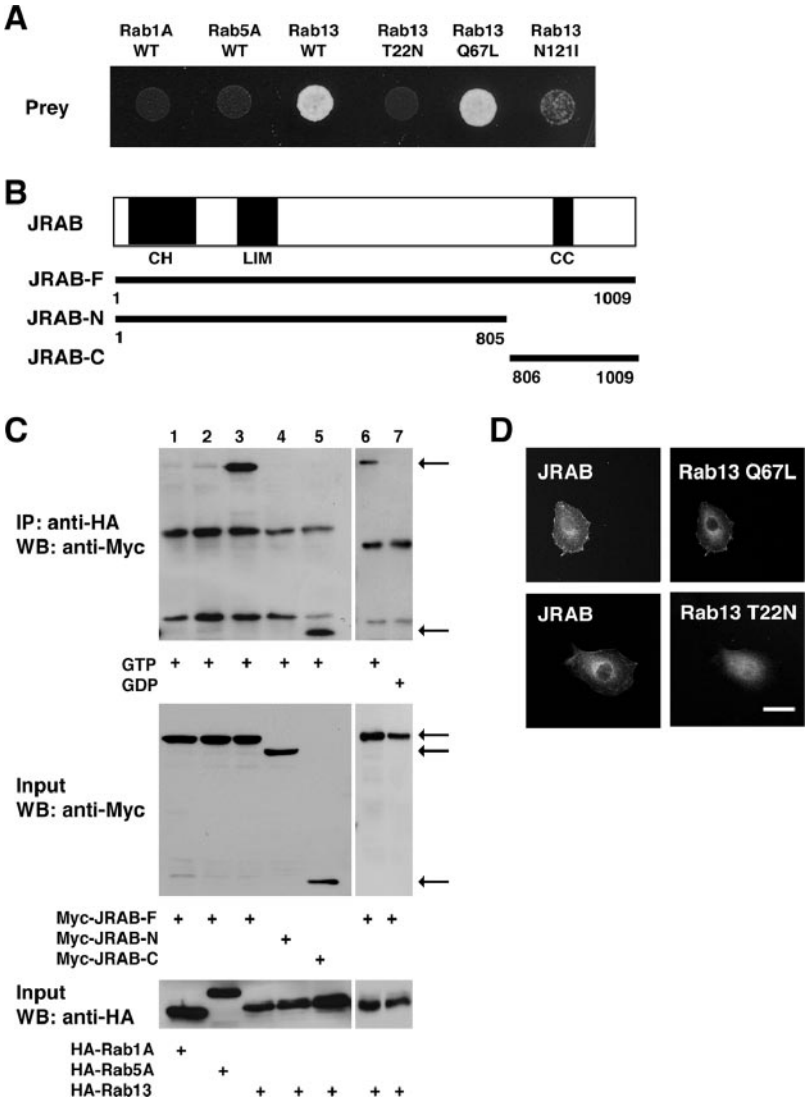

Figure 1. Binding of JRAB to Rab13. (A)Yeast transformants carrying the prey vector pACT2 encoding clone TTY124 and pGBDU vector encoding Rab1A WT, Rab5A WT, Rab13 WT, Rab13 T22N, Rab13 Q67L, or Rab13 N121I were spotted on synthetic complete medium lacking adenine to score for ADE2 reporter activity and incubated at 30°C for 3 d. (B) Structures of the full length and various fragments of JRAB. CH, calponin homology domain; LIM, LIM domain; CC, coiled-coil domain. (C) BHK cells were cotransfected with pCI-neo-Myc vector encoding JRAB-F, JRAB-N, or JRAB-C and pCI-neo-HA vector encoding Rab1A, Rab5A, or Rab13 as indicated. BHK cell extracts were immunoprecipitated (IP) with an anti-HA antibody and analyzed by Western blot (WB) with anti-Myc and anti-HA antibodies. The arrows indicate JRAB-F, JRAB-N, and JRAB-C. (D) BHK cells were cotransfected with pCI-neo-Myc-JRAB-F and either pCI-neo-HA-Rab13 T22N or pCI-neo-HA-Rab13 Q67L and were subjected to immunofluorescence microscopy using anti-Myc and anti-HA antibodies. Bar, 20 μm. The results shown in A, C, and D are representative of three independent experiments.

nolabeling of JRAB with Rab13 Q67L and Rab13 T22N in BHK cells. When Myc-JRAB and HA-Rab13 Q67L were cotransfected into BHK cells, they were colocalized to the PM and the perinuclear region (Figure 1D). In contrast, Myc-JRAB showed a staining pattern distinct from Rab13 T22N and was localized to the PM in BHK cells cotransfected with Myc-JRAB and HA-Rab13 T22N (Figure 1D). These results indicate that JRAB specifically interacts with the GTP-bound form of Rab13.

JRAB Is Expressed in Epithelial Tissues and Localized to TJs in MTD-1A Cells

To gain insight into the physiological function of JRAB, we generated a rat anti-JRAB antibody. This antibody recognized a single ~110-kDa protein, matching the 108.2-kDa size calculated from the JRAB cDNA sequence, in mouse brain, lung, liver, and kidney (Figure 2A). Epithelial MTD-1A cells as well as fibroblastic NIH3T3 and L cells were also found to express the ~110-kDa JRAB protein (Figure 2A). These results indicate that JRAB protein is expressed in epithelial tissues and both epithelial and fibroblastic cells, where Rab13 is also expressed (Zahraoui *et al*., 1994).

To determine the intracellular localization of JRAB, we first carried out the subcellular fractionation of MTD-1A cells. The PNS and the resulting supernatant (S100) and pellet (P100) fractions were subjected to Western blot analysis with anti-JRAB, anti-ZO-1, and anti-occludin antibodies. Although occludin, which possesses four transmembrane domains, was detected exclusively in the P100 fraction, ZO-1, which bears no transmembrane domains, was localized to both the S100 and P100 fractions (Figure 2B). Like ZO-1, JRAB was also present in both S100 and P100 fractions. We next performed double immunolabeling of JRAB with ZO-1 in MTD-1A cells grown on filters. JRAB was detected both in the cell–cell contacts of the PM, where it was mostly colocalized with ZO-1, and in the cytosol of polarized MTD-1A cells (Figure 2C). A vertical section of a confocal image revealed that JRAB as well as ZO-1 was present at apical side of cell–cell contacts (Figure 2C). Together, these results suggest that a considerable part of JRAB protein is localized to TJs in MTD-1A cells.

JRAB Mediates the Endocytic Recycling of Occludin in MTD-1A Cells

If JRAB is localized to TJs and interacts with the GTP-bound form of Rab13 in MTD-1A cells, it would mediate the endocytic recycling of occludin but not TfR (Morimoto *et al*., 2005). Thus, we examined the effect of Myc-JRAB-F, Myc-

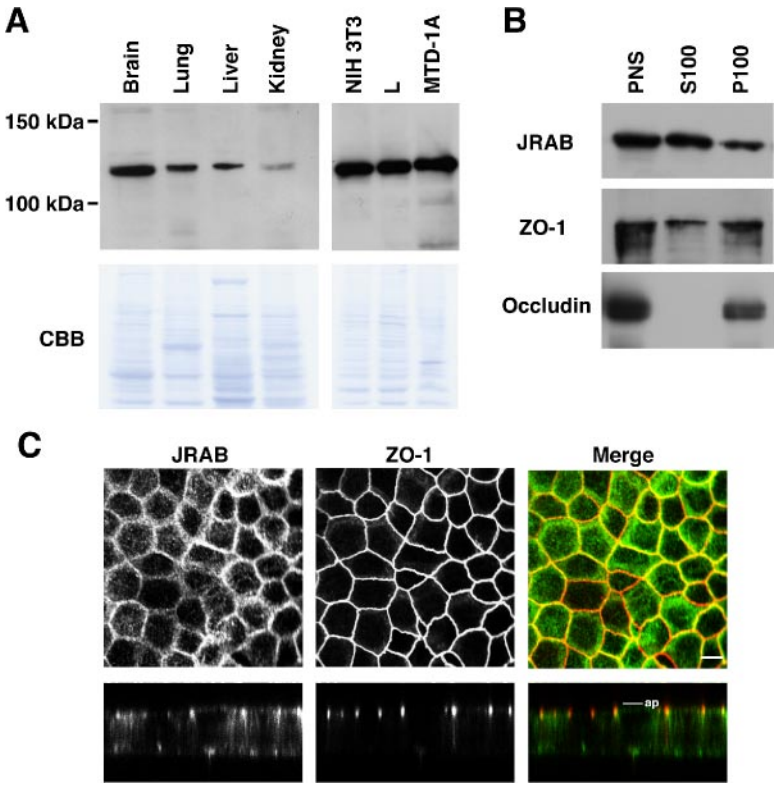

Figure 2. Expression and localization of JRAB. (A) Homogenates of the indicated mouse tissues and cells (30 μg of protein each) were subjected to SDS-PAGE, followed by Western blot with an anti-JRAB antibody. The PVDF membranes stained with Coomassie brilliant blue (CBB) are presented in the bottom panels. (B) Subcellular fractionation of MTD-1A cells was performed and the indicated fractions were subjected to SDS-PAGE, followed by Western blot with an anti-JRAB antibody. (C) MTD-1A cells were double immunostained with anti-JRAB and anti-ZO-1 antibodies and observed under a confocal microscope. Vertical sectional images were generated and shown in the bottom panels. In the merged images, JRAB was green and ZO-1 was red. Bars, 10 μm. ap, level of apical membranes. The results shown are representative of three independent experiments.

JRAB-N, and Myc-JRAB-C on the endocytic recycling of occludin and TfR. For this purpose, we performed a biochemical recycling assay based on cell surface biotinylation, in which a decrease in biotinylated cargo molecules represents their recycling back to the cell surface as described previously (Morimoto *et al*., 2005). When MTD-1A cells were infected with Ad-Myc-JRAB-F or Ad-Myc-JRAB-C, the recycling of occludin was comparable with that in Ad-EGFP–infected MTD-1A cells (Figure 3A). In contrast, the recycling of occludin in Ad-Myc-JRAB-N–infected cells was inhibited as potently as in Ad-EGFP-Rab13 Q67L-infected cells (Figure 3A). The recycling of TfR in MTD-1A cells was not affected by the expression of Myc-JRAB-F, Myc-JRAB-N, Myc-JRAB-C, or EGFP-Rab13 Q67L (Figure 3A).

Because Rab13 Q67L selectively inhibited the recycling, but not the endocytosis, of occludin in MTD-1A cells, we

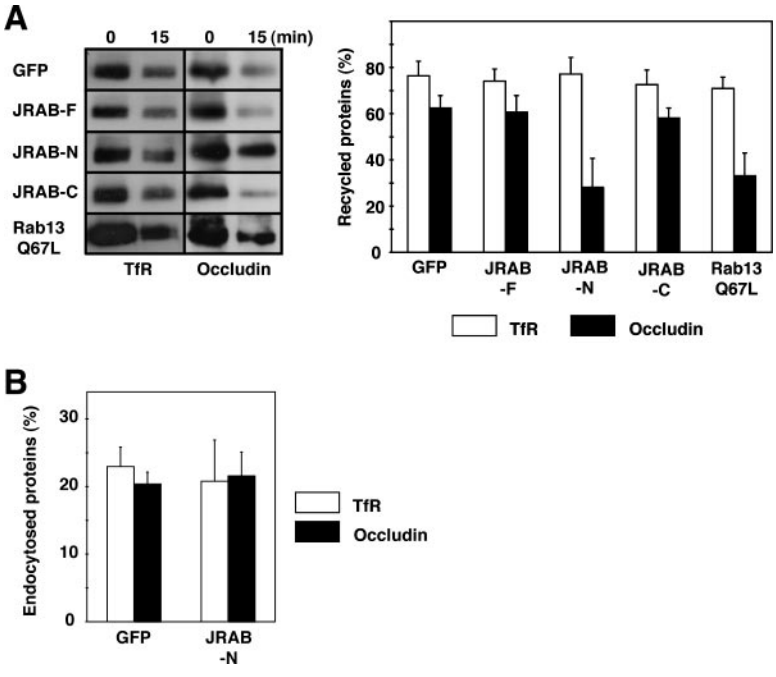

Figure 3. Involvement of JRAB in the endocytic recycling of occludin in MTD-1A cells. (A) MTD-1A cells infected with Ad-EGFP (GFP), Ad-Myc-JRAB-F (JRAB-F), Ad-Myc-JRAB-N (JRAB-N), Ad-Myc-JRAB-C (JRAB-C), or Ad-EGFP-Rab13 Q67L (Rab13 Q67L) were cell surface biotinylated and incubated at 37°C for 15 min to allow for endocytosis of biotinylated occludin or TfR on the cell surface. After stripping the remaining biotin from the cell surface, cells were again incubated at 37°C for 15 min to allow recycling of biotinylated occludin or TfR back to the cell surface. After a second stripping of cell surface biotin, biotinylated occludin or TfR was isolated with avidin beads and quantitated by Western blot with anti-occludin or anti-TfR antibody. Recycled proteins represent the percentage of endocytosed proteins and expressed as the mean and SEM of three independent experiments. (B) MTD-1A cells infected with Ad-EGFP (GFP) or Ad-Myc-JRAB-N (JRAB-N) were cell surface biotinylated and incubated at 37°C for 15 min to allow for endocytosis of biotinylated occludin or TfR on the cell surface. After stripping the remaining biotin from the cell surface, biotinylated occludin or TfR was isolated and quantitated. Endocytosed proteins represent the percentage of endocytosed proteins and expressed as the mean and SEM of three independent experiments.

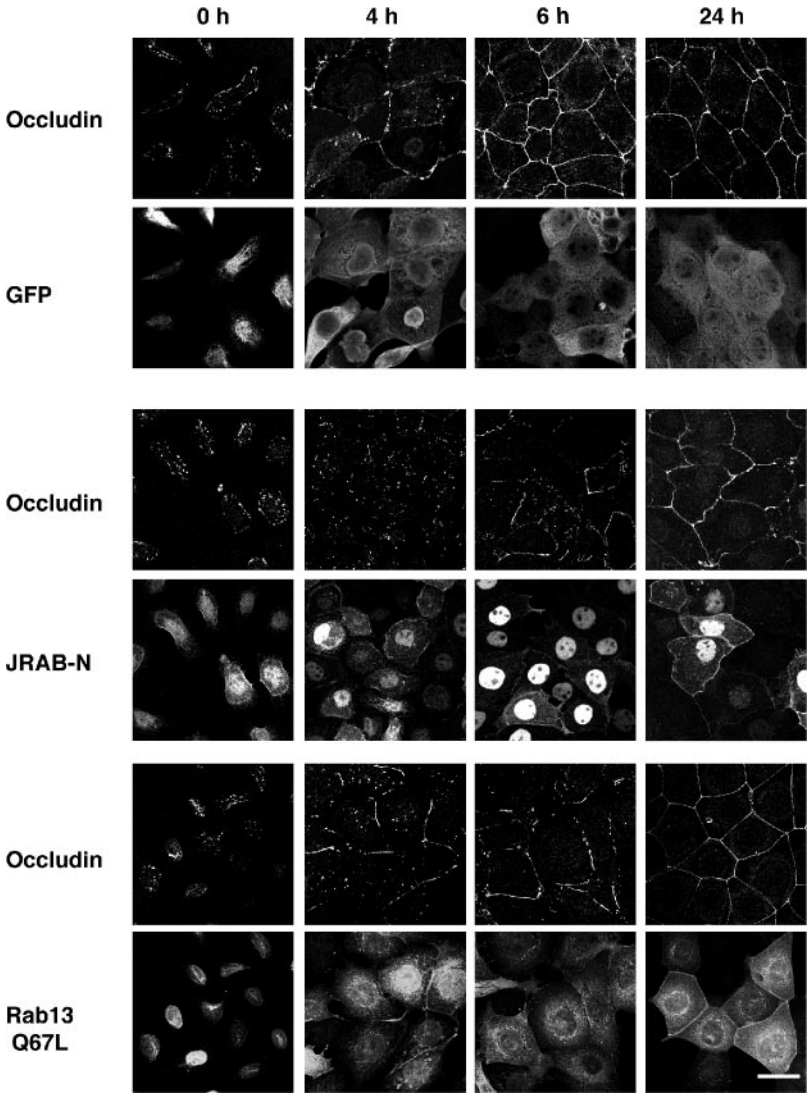

Figure 4. Involvement of JRAB in the recruitment of occludin to the PM during Ca^{2+} switch in MTD-1A cells. MTD-1A cells infected with Ad-EGFP (GFP), Ad-Myc-JRAB-N (JRAB-N), or Ad-EGFP-Rab13 Q67L (Rab13 Q67L) were subjected to the Ca^{2+} switch assay, and were then double immunostained with anti-occludin and anti-GFP antibodies at 0, 4, 6, and 24 h after Ca^{2+} restoration. Bar, 20 μm. The results shown are representative of three independent experiments.

next investigated the effect of JRAB-N on its endocytosis using a biochemical endocytosis assay as described previously (Morimoto *et al*., 2005). The endocytosis of occludin as well as TfR in Ad-Myc-JRAB-N-infected MTD-1A cells was comparable with that in Ad-EGFP–infected cells (Figure 3B), suggesting that JRAB did not mediate the endocytosis of occludin. Together, these results indicated that JRAB and Rab13 specifically regulated the endocytic recycling of occludin in MTD-1A cells.

JRAB and Rab13 Direct the Recruitment of Occludin to the PM during Ca^{2+} Switch in MTD-1A Cells

To further characterize the action of JRAB-N, we examined the intracellular localization of occludin in MTD-1A cells using a Ca^{2+} switch assay (Kartenbeck *et al*., 1991). MTD-1A cells were incubated in Ca^{2+}-chelated medium to dissociate cell–cell junctions. Subsequently, physiological Ca^{2+} was restored, resulting in the synchronous assembly of cell–cell junctions. Occludin localization was then analyzed by immunofluorescence microscopy at 0, 4, 6, and 24 h after induction of cell–cell contacts. In MTD-1A cells infected with Ad-EGFP, Ad-Myc-JRAB-N, or Ad-EGFP-Rab13 Q67L, removal of Ca^{2+} resulted in immediate dissociation of occludin from the PM with intracellular accumulation (Figure 4, 0 h). Within 24 h after Ca^{2+} restoration, intracellular occludin staining was absent and PM staining was observed to be continuous in all cases (Figure 4, 24 h). However, the kinetics of recruitment of occludin to the PM seemed dissimilar. In GFP-expressing MTD-1A cells, disappearance of intracellular occludin signal and continuous staining of the PM was observed as soon as 6 h after Ca^{2+} restoration (Figure 4, 6 h). In contrast, continuous staining of the PM was much delayed in JRAB-N- and Rab13 Q67L-expressing MTD-1A cells (Figure 4, 6 h), indicating that JRAB as well as Rab13 direct the recruitment of occludin to the PM during Ca^{2+} switch in MTD-1A cells.

JRAB and Rab13 Mediate the Assembly of Functional TJs during Ca^{2+} Switch in MTD-1A Cells

We next investigated the effect of JRAB-N on the formation of functional TJs. TJs seal the PMs of adjacent cells to form an intact epithelial sheet. TER can be used to monitor the tightness of the seal. When expressed after the completed formation of functional TJs, there was no observable difference between the TER of cells expressing GFP and JRAB-N (our unpublished data). We then tested the effect of JRAB-N

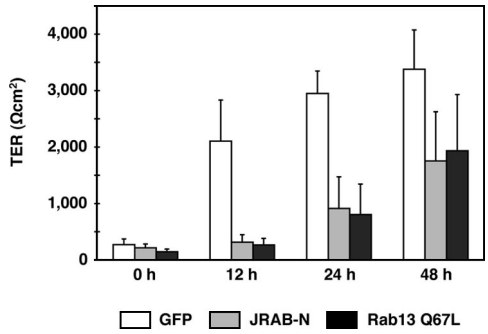

Figure 5. Involvement of JRAB in the development of TER during Ca^{2+} switch in MTD-1A cells. MTD-1A cells expressing GFP (GFP), Myc-tagged JRAB-N (JRAB-N), or GFP-tagged Rab13 Q67L (Rab13 Q67L) were subjected to Ca^{2+} switch assay. TER was measured at 0, 12, 24, and 48 h after Ca^{2+} restoration. The results shown are the mean and SEM of three independent experiments performed in duplicate.

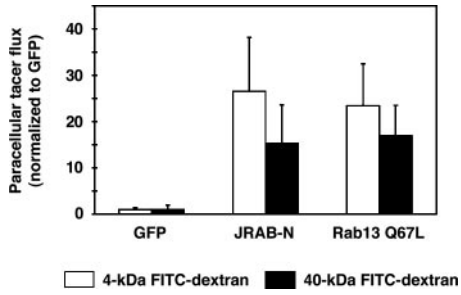

Figure 6. Involvement of JRAB in the formation of paracellular diffusion barrier during Ca^{2+} switch in MTD-1A cells. MTD-1A cells expressing GFP (GFP), Myc-tagged JRAB-N (JRAB-N), or GFP-tagged Rab13 Q67L (Rab13 Q67L) were subjected to Ca^{2+} switch assay. Paracellular fluxes of 4- and 40-kDa FITC-dextran were measured at 12 h after Ca^{2+} restoration. The amount of tracer diffusion is normalized to that of GFP-expressing MTD-1A cells. The results shown are the mean and SEM of three independent experiments performed in duplicate.

expression on TJ assembly using the Ca^{2+} switch assay. MTD-1A cells expressing GFP, JRAB-N, or Rab13 Q67L all went from the same maximal TER (>3000 Ωcm^2) to the same minimal TER (10–20 Ωcm^2) after incubation in Ca^{2+}-chelated medium (Figure 5). Subsequent incubation in physiological Ca^{2+} medium triggered a time-dependent increase in TER, which was measured at 0, 12, 24, and 48 h. MTD-1A cells expressing JRAB-N exhibited a significantly delayed increase in TER compared with GFP-expressing MTD-1A cells (Figure 5). Rab13 Q67L also slowed the development of TER as described previously (Marzesco *et al*., 2002).

Because TJs serve as a selective barrier to diffusion across an epithelial sheet, we further examined the effect of JRAB-N on the diffusion of membrane-impermeable paracellular tracers (4- and 40-kDa FITC-dextran) across monolayer of MTD-1A cells. When paracellular tracer flux was measured after completed TJ development, there was no observable difference between MTD-1A cells expressing GFP, JRAB-N, or Rab13 Q67L (our unpublished data). Paracellular tracer flux was then measured during TJ assembly using the Ca^{2+} switch assay. Paracellular flux of 4- and 40-kDa FITC-dextran was measured 12 h after restoration of physiological Ca^{2+}, when the delay in TER development of JRAB-N– and Rab13 Q67L-expressing MTD-1A cells was most evident (Figure 5). Compared with GFP-expressing MTD-1A cells, the expression of JRAB-N permitted ~26- and ~15-fold increases in the paracellular flux of 4- and 40-kDa FITC-dextran, respectively (Figure 6). Consistent with a previous report (Marzesco *et al*., 2002), MTD-1A cells expressing Rab13 Q67L also showed a similar increase in 4- and 40-kDa FITC-dextran paracellular flux (Figure 6). These results suggest that JRAB as well as Rab13 mediate the assembly of functional TJs during Ca^{2+} switch in MTD-1A cells.

Actin Filament Is Important for JRAB Localization to TJs

To explore the molecular mechanisms of JRAB action, we investigated the requirements for JRAB localization to TJs. First, we examined the interaction between JRAB and Rab13 in MTD-1A cells. Although the anti-JRAB antibody detected the endogenous protein, our antibody against Rab13 did not yield reliable signal for the endogenous protein in MTD-1A cells. We therefore expressed HA-Rab13 WT in MTD-1A cells and analyzed its binding to endogenous JRAB by coimmunoprecipitation. When HA-Rab13 WT or HA-vector was transfected into MTD-1A cells, endogenous JRAB was specifically coimmunoprecipitated with HA-Rab13 but not HA-vector (Figure 7A), suggesting that JRAB could physiologically interacted with Rab13 in MTD-1A cells.

Because many Rab-binding proteins were recruited by the GTP-bound form of Rab to the membrane where Rab resided, we next assessed whether Rab13 was important for JRAB localization to TJs. For this purpose, we cotransfected Myc-JRAB-F with HA-Rab13 WT, HA-Rab13 T22N, HA-Rab13 Q67L, or HA-Rab13 N121I into MTD-1A cells and analyzed the localization of proteins by immunofluorescence microscopy. Myc-JRAB-F was colocalized to a large extent with HA-Rab13 WT and HA-Rab13 Q67L in the PM and the perinuclear region (Figure 7B). In contrast, Myc-JRAB-F was targeted to the PM and the perinuclear region, whereas HA-Rab13 T22N and HA-Rab13 N121I were typically distributed to the cytosol (Figure 7B). Importantly, Myc-JRAB-F was associated with the PM irrespective of the guanine nucleotide status of transfected Rab13. Then, we determined the localization of Myc-JRAB-F, Myc-JRAB-N, and Myc-JRAB-C expressed in MTD-1A cells. Whereas Myc-JRAB-N, which did not bind to Rab13, was targeted to the PM, Myc-JRAB-C, which efficiently bound to Rab13, yielded a cytosolic localization (Figure 7C). These results indicated that Rab13 is not essential for JRAB localization to TJs.

Because JRAB contained CH and LIM domains implicated in the association with actin cytoskeleton, we next examined whether JRAB localization to TJs depended on the integrity of actin cytoskeleton. When we treated MTD-1A cells with cytochalasin D, which depolymerized F-actin by capping its barbed ends, F-actin was disrupted and localized in focal accumulation along the PM and in aggregates throughout the cytosol as described previously (Stevenson and Begg, 1994) (Figure 7D). Although JRAB was targeted to the PM in control cells, it was displaced from the PM in cytochalasin D-treated cells, suggesting that the integrity of actin cytoskeleton was required for JRAB localization to TJs (Figure 7D). Because many TJ components were displaced from the PM by actin depolymerization, we next looked for the colocalization of JRAB with actin cytoskeleton (Stevenson and Begg, 1994; Ivanov *et al*., 2004a, 2005a). Although endogenous JRAB colocalized with a circumferential actin belt in control cells (Figure 7D, arrow), Ca^{2+} depletion revealed its colocalization with an actin ring and radiating actin cables (Figure 7E, arrow). Furthermore, endogenous JRAB was also distributed along stress fibers in NIH3T3 cells (Figure 7F,

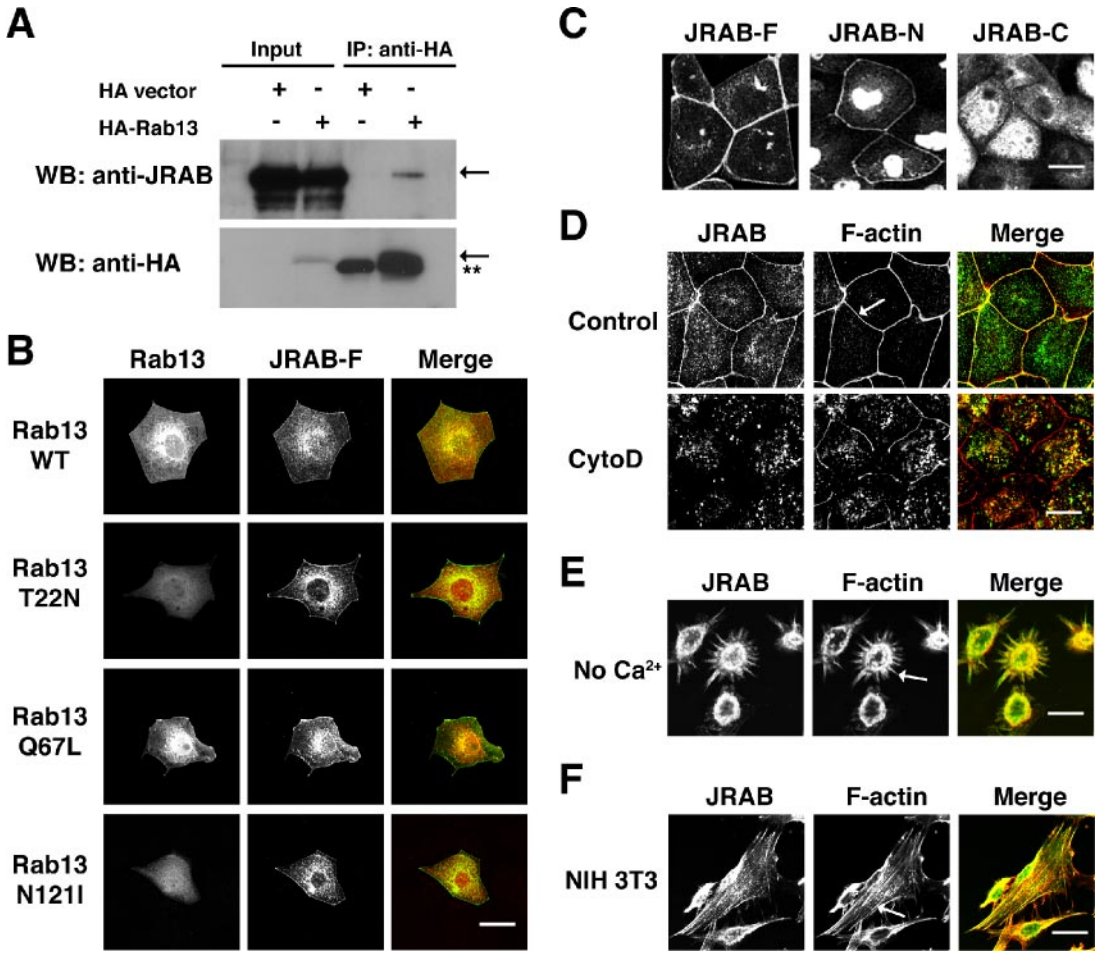

Figure 7. Requirement of JRAB localization to TJs. (A) MTD-1A cells were transfected with pCI-neo-HA-Rab13 WT, immunoprecipitated (IP) with an anti-HA antibody, and analyzed by Western blot (WB) with anti-JRAB and anti-HA antibodies. The arrows indicate endogenous JRAB and HA-Rab13 WT. The double stars indicate the Ig light chain. (B) MTD-1A cells were cotransfected with pCI-neo-Myc-JRAB-F and pCI-neo-HA-Rab13 WT, pCI-neo-HA-Rab13 T22N, pCI-neo-HA-Rab13 Q67L, or pCI-neo-HA-Rab13 N121I and were subjected to immunofluorescence microscopy using anti-Myc and anti-HA antibodies. In the merged images, JRAB was green and Rab13 was red. Bar, 20 μm. (C) MTD-1A cells were infected with Ad-Myc-JRAB-F (JRAB-F), Ad-Myc-JRAB-N (JRAB-N), or Ad-Myc-JRAB-C (JRAB-C) and subjected to immunofluorescence microscopy using an anti-Myc antibody. Bar, 20 μm. (D) MTD-1A cells were incubated for 2 h in the absence (control) or presence of 10 μM cytochalasin D (CytoD) and double labeled with anti-JRAB antibody and rhodamine-phalloidin. The arrow indicates a circumferential actin belt. In the merged images, JRAB was green and F-actin was red. Bar, 20 μm. (E) MTD-1A cells were incubated in Ca^{2+}-chelated medium for 60 min and double-labeled with anti-JRAB antibody and rhodamine-phalloidin. The arrow indicates radiating actin cables. In the merged images, JRAB was green and F-actin was red. Bar, 20 μm. (F) NIH3T3 cells were double labeled with anti-JRAB antibody and rhodamine-phalloidin. The arrow indicates stress fibers. In the merged images, JRAB was green and F-actin was red. Bar, 10 μm. The results shown in A–F are representative of three independent experiments.

arrow). Together, these results suggested that JRAB was directly or indirectly associated with actin cytoskeleton.

DISCUSSION

Dynamic turnover of TJs is required for EMT and/or MET, which are fundamental processes underlying epithelial morphogenesis in multicellular organisms as well as a variety of diseases, including renal fibrosis and tumor metastasis (Schock and Perrimon, 2002; Thiery, 2003). To begin to address the molecular mechanisms of dynamic turnover of TJs, we investigated the intracellular transport of occludin and claudins to and from the cell surface and found that occludin was subject to the endocytic recycling. We further identified Rab13 as its crucial regulator (Yamamoto *et al*., 2003; Morimoto *et al*., 2005). In the present study, we have isolated and characterized JRAB as a novel Rab13-binding protein that localized to TJs and controlled the endocytic recycling of occludin as well as the formation of functional TJs.

Now, accumulating evidence indicates that the endocytic transport of TJ proteins is implicated in a rapid turnover of TJs (Ivanov *et al*., 2005b). Although the coendocytosis of claudins on the two apposed PMs into one of the adjacent cells was detected during the intercellular movement of epithelial cells, we here characterized the endocytic recycling of occludin in contacting and Ca^{2+}-switched epithelial cells (Matsuda *et al*., 2004; Morimoto *et al*., 2005). Although the coendocytosis of transinteracting occludin on the two apposed PMs could also occur, the intracellular occludin was segregated from the co-endocytosed claudins (Matsuda *et al*., 2004). In addition to the coendocytosis, recent studies revealed three mechanisms for occludin endocytosis in different cellular conditions. Clathrin-

dependent endocytosis in Ca^{2+}-depleted intestinal epithelial T84 cells, caveolin-dependent endocytosis in *E. coli* cytotoxic necrotizing factor-1–treated T84 cells and actin-depolymerized kidney epithelial MDCK cells, and macropinocytosis in interferon-γ-treated T84 cells were identified and characterized for a mechanism of occludin endocytosis (Hopkins *et al*., 2003; Ivanov *et al*., 2004b; Bruewer *et al*., 2005; Shen and Turner, 2005). We should determine the functional role of each occludin–endocytosis pathway under physiological and pathological conditions in the future.

As to the destinations of endocytosed TJ proteins, early endosomal antigen 1-positive early endosomes, Rab11-positive recycling endosomes, Rab7-positive late endosomes, Rab13-positive vesicles, Syntaxin4-positive compartment, and Syntaxin3-positive vacuolar apical compartment were identified (Harhaj *et al*., 2002; Hopkins *et al*., 2003; Ivanov *et al*., 2004b; Matsuda *et al*., 2004; Bruewer *et al*., 2005; Morimoto *et al*., 2005; Utech *et al*., 2005). Although the endocytosed occludin in Rab7-positive late endosomes was likely targeted to lysosomal degradation, it was possibly recycled back to the PM. Although occludin was reported to be accumulated in Syntaxin4-positive compartment in Ca^{2+}-depleted epithelial cells (Ivanov *et al*., 2004b), we showed that endocytosed occludin was recycled back to the PM in a Rab13- and JRAB-dependent manner during Ca^{2+} switch. Considering that a single Rab protein can regulate multiple biochemical reactions at distinct sites, Rab13 and JRAB may work at Syntaxin4-positive compartment, recycling vesicles containing occludin, and/or PM (Takai *et al*., 2001; Zerial and McBride, 2001; Pfeffer and Aivazian, 2004; Seabra and Wasmeier, 2004). It will be of interest in future studies to define the sites for Rab13-JRAB action.

Although we identified JRAB as a Rab13-binding protein, it was originally identified in the GenBank/EMBL/DDBJ Data Bank as being related to MICAL, which contains a monooxygenase domain, a CH domain, a LIM domain, a proline-rich region, and a CC domain (Suzuki *et al*., 2002; Terman *et al*., 2002). MICAL interacts directly with the Src homology 3 domain of the adaptor protein CasL/HEF1/NEDD9, which played an important role in cytoskeletal regulation and cell migration, via its proline-rich PPKPP sequence. It also binds to the cytoplasmic domain of plexins, which serve as signal-transducing receptors for semaphorins, via its C terminus containing the CC domain (Terman *et al*., 2002). In contrast to the interaction of MICAL with Rab1 (Weide *et al*., 2003), JRAB was associated with Rab13 but not Rab1. Although intermediate filaments and microtubules were identified as MICAL-associated cytoskeletons (Suzuki *et al*., 2002; Fischer *et al*., 2005), actin cytoskeleton was directly or indirectly associated with JRAB. Together, it is likely that JRAB as well as MICAL functions as the protein-binding scaffolds and interacts with a number of other proteins that await discovery.

Activation of Rab protein by GEP generally leads to the recruitment of Rab-binding proteins to the membrane where Rab protein resides. This condition can be enhanced by overexpression of wild type or dominant active mutant of Rab protein, whereas overexpression of dominant negative or empty mutant causes Rab-binding proteins to localize in the cytosol (Takai *et al*., 2001; Zerial and McBride, 2001; Pfeffer and Aivazian, 2004; Seabra and Wasmeier, 2004). Neither of these phenotypes was observed for Rab13 and JRAB. Transfected JRAB associated with the PM in the presence of any of transfected Rab13 mutant. In agreement with this, JRAB-N lacking the Rab13-binding domain was localized to the PM. Interestingly, Rab27 and Munc13-4, which were localized to secretory vesicles, also showed the same phenotypes as Rab13 and JRAB (Neeft *et al*., 2005). It will be important to clarify exact molecular mechanisms for these Rab-binding proteins to recognize the specific sites of intracellular membranes in the future.

In the present study, we showed that JRAB was directly or indirectly associated with F-actin. This interaction had a potential impact on Rab13 and TJs function. With regard to Rab13 function, an increasing number of Rab-binding proteins were known to be directly or indirectly associated with actin cytoskeleton (Kato *et al*., 1996; Fukuda and Kuroda, 2002; Hales *et al*., 2002; Strom *et al*., 2002; Lanzetti *et al*., 2004; Sahlender *et al*., 2005). As a Rab13-binding protein, JRAB may link occludin-containing vesicles to actin cytoskeleton (Jordens *et al*., 2005). With regard to TJs function, it is well known that TJs physically and functionally associated with a circumferential actin belt and contained a number of actin-binding proteins, including occludin, ZO family proteins, cingulin, and JACOP (Wittchen *et al*., 1999; D'Atri and Citi, 2001; Vasioukhin and Fuchs, 2001; Bershadsky, 2004; Ohnishi *et al*., 2004). Like ZO family proteins, JRAB may link TJs to a circumferential actin belt and control the formation of functional TJs.

As a next step to understand the molecular mechanism of dynamic turnover of TJs, we should elucidate the physiological significance of Rab13- and JRAB-dependent recycling of occludin. Whereas occludin was the first integral TJ protein to be identified, its deletion from embryonic stem cells did not prevent differentiation of these cells into polarized epithelial cells with clear TJs (Furuse *et al*., 1993; Saitou *et al*., 1998). However, endocytosis of occludin was correlated with TJs structural and functional disruption induced by actin depolymerization with latrunculin A (Shen and Turner, 2005). Depletion of occludin by RNA interference in MDCK cells revealed that occludin transduced signals from apoptotic cells to the actin cytoskeleton via a Rho signaling pathway (Yu *et al*., 2005). Occludin was also shown to regulate transforming growth factor (TGF)-β receptor localization for efficient TGF-β-dependent turnover of TJs during EMT (Barrios-Rodiles *et al*., 2005). It is still premature to discuss further the relationship of this putative occludin signaling with the endocytic recycling of occludin, but through a sophisticated mechanism, epithelial cells would coordinate many signals to dynamically reorganize TJs during epithelial morphogenesis.

In summary, the present study demonstrates that JRAB interacts with GTP-bound form of Rab13 and regulates the endocytic recycling of occludin as well as the formation of functional TJs. The mechanism of JRAB action involves its direct or indirect association with actin cytoskeleton, which could functionally link Rab13 to actin cytoskeleton.

ACKNOWLEDGMENTS

We thank Drs. S. Tsukita and M. Furuse (Kyoto University) for MTD-1A cells, L cells, anti-occludin (MOC37) antibody, and valuable discussion; and Dr. N. Sakai (Hiroshima University, Hiroshima, Japan) for helpful suggestions regarding the construction of recombinant adenovirus. This study was supported by Grants-in-Aid for Scientific Research 16590231 (to N. N.) and 15079207 (to T. S.) from the Ministry of Education, Science, Sports, Culture and Technology of Japan. The nucleotide sequence reported in this article has been submitted to the GenBank/EMBL/DDBJ Data Bank with accession number AB182579.

REFERENCES

Anderson, J. M., Van Itallie, C. M., and Fanning, A. S. (2004). Setting up a selective barrier at the apical junction complex. Curr. Opin. Cell Biol. *16*, 140–145.

Barrios-Rodiles, M., *et al*. (2005). High-throughput mapping of a dynamic signaling network in mammalian cells. Science *307*, 1621–1625.

Bershadsky, A. (2004). Magic touch: how does cell-cell adhesion trigger actin assembly? Trends Cell Biol. *14*, 589–593.

Bruewer, M., Utech, M., Ivanov, A. I., Hopkins, A. M., Parkos, C. A., and Nusrat, A. (2005). Interferon-γ induces internalization of epithelial tight junction proteins via a macropinocytosis-like process. FASEB J. *19*, 923–933.

D'Atri, F., and Citi, S. (2001). Cingulin interacts with F-actin in vitro. FEBS Lett. *507*, 21–24.

Di Giovanni, S., De Biase, A., Yakovlev, A., Finn, T., Beers, J., Hoffman, E. P., and Faden, A. I. (2005). In vivo and in vitro characterization of novel neuronal plasticity factors identified following spinal cord injury. J. Biol. Chem. *280*, 2084–2091.

Fischer, J., Weide, T., and Barnekow, A. (2005). The MICAL proteins and rab 1, a possible link to the cytoskeleton? Biochem. Biophys. Res. Commun. *328*, 415–423.

Fukuda, M., and Kuroda, T. S. (2002). Slac2-c (synaptotagmin-like protein homologue lacking C2 domains-c), a novel linker protein that interacts with Rab27, myosin Va/VIIa, and actin. J. Biol. Chem. *277*, 43096–43103.

Furuse, M., Fujita, K., Hiiragi, T., Fujimoto, K., and Tsukita, S. (1998a). Claudin-1 and -2, novel integral membrane proteins localizing at tight junctions with no sequence similarity to occludin. J. Cell Biol. *141*, 1539–1550.

Furuse, M., Hirase, T., Itoh, M., Nagafuchi, A., Yonemura, S., and Tsukita, S. (1993). Occludin: a novel integral membrane protein localizing at tight junctions. J. Cell Biol. *123*, 1777–1788.

Furuse, M., Sasaki, H., Fujimoto, K., and Tsukita, S. (1998b). A single gene product, claudin-1 or -2, reconstitutes tight junction strands and recruits occludin in fibroblasts. J. Cell Biol. *143*, 391–401.

Hales, C. M., Vaerman, J. P., and Goldenring, J. R. (2002). Rab11 family interacting protein 2 associates with Myosin Vb and regulates plasma membrane recycling. J. Biol. Chem. *277*, 50415–50421.

Harhaj, N. S., Barber, A. J., and Antonetti, D. A. (2002). Platelet-derived growth factor mediates tight junction redistribution and increases permeability in MDCK cells. J. Cell Physiol. *193*, 349–364.

Hopkins, A. M., Walsh, S. V., Verkade, P., Boquet, P., and Nusrat, A. (2003). Constitutive activation of Rho proteins by CNF-1 influences tight junction structure and epithelial barrier function. J. Cell Sci. *116*, 725–742.

Ivanov, A. I., Hunt, D., Utech, M., Nusrat, A., and Parkos, C. A. (2005a). Differential roles for actin polymerization and a myosin II motor in assembly of the epithelial apical junctional complex. Mol. Biol. Cell *16*, 2636–2650.

Ivanov, A. I., McCall, I. C., Parkos, C. A., and Nusrat, A. (2004a). Role for actin filament turnover and a myosin II motor in cytoskeleton-driven disassembly of the epithelial apical junctional complex. Mol. Biol. Cell *15*, 2639–2651.

Ivanov, A. I., Nusrat, A., and Parkos, C. A. (2004b). Endocytosis of epithelial apical junctional proteins by a clathrin-mediated pathway into a unique storage compartment. Mol. Biol. Cell *15*, 176–188.

Ivanov, A. I., Nusrat, A., and Parkos, C. A. (2005b). Endocytosis of the apical junctional complex: mechanisms and possible roles in regulation of epithelial barriers. Bioessays *27*, 356–365.

James, P., Halladay, J., and Craig, E. A. (1996). Genomic libraries and a host strain designed for highly efficient two-hybrid selection in yeast. Genetics *144*, 1425–1436.

Jordens, I., Marsman, M., Kuijl, C., and Neefjes, J. (2005). Rab proteins, connecting transport and vesicle fusion. Traffic *6*, 1070–1077.

Kaiser, C., Michaelis, S., and Mitchell, A. (eds.) (1994). Methods in Yeast Genetics, Cold Spring Harbor, NY: Cold Spring Harbor Laboratory Press.

Kartenbeck, J., Schmelz, M., Franke, W. W., and Geiger, B. (1991). Endocytosis of junctional cadherins in bovine kidney epithelial (MDBK) cells cultured in low Ca^{2+} ion medium. J. Cell Biol. *113*, 881–892.

Kato, M., Sasaki, T., Ohya, T., Nakanishi, H., Nishioka, H., Imamura, M., and Takai, Y. (1996). Physical and functional interaction of rabphilin-3A with α-actinin. J. Biol. Chem. *271*, 31775–31778.

Kohler, K., Louvard, D., and Zahraoui, A. (2004). Rab13 regulates PKA signaling during tight junction assembly. J. Cell Biol. *165*, 175–180.

Lanzetti, L., Palamidessi, A., Areces, L., Scita, G., and Di Fiore, P. P. (2004). Rab5 is a signalling GTPase involved in actin remodelling by receptor tyrosine kinases. Nature *429*, 309–314.

Lawrence, D. W., Comerford, K. M., and Colgan, S. P. (2002). Role of VASP in reestablishment of epithelial tight junction assembly after Ca^{2+} switch. Am. J. Physiol. *282*, C1235–C1245.

Le, T. L., Yap, A. S., and Stow, J. L. (1999). Recycling of E-cadherin: a potential mechanism for regulating cadherin dynamics. J. Cell Biol. *146*, 219–232.

Marzesco, A. M., Dunia, I., Pandjaitan, R., Recouvreur, M., Dauzonne, D., Benedetti, E. L., Louvard, D., and Zahraoui, A. (2002). The small GTPase Rab13 regulates assembly of functional tight junctions in epithelial cells. Mol. Biol. Cell *13*, 1819–1831.

Matsuda, M., Kubo, A., Furuse, M., and Tsukita, S. (2004). A peculiar internalization of claudins, tight junction-specific adhesion molecules, during the intercellular movement of epithelial cells. J. Cell Sci. *117*, 1247–1257.

Morimoto, S., Nishimura, N., Terai, T., Manabe, S., Yamamoto, Y., Shinahara, W., Miyake, H., Tashiro, S., Shimada, M., and Sasaki, T. (2005). Rab13 mediates the continuous endocytic recycling of occludin to the cell surface. J. Biol. Chem. *280*, 2220–2228.

Neeft, M., *et al*. (2005). Munc13-4 is an effector of rab27a and controls secretion of lysosomes in hematopoietic cells. Mol. Biol. Cell *16*, 731–741.

Ohnishi, H., Nakahara, T., Furuse, K., Sasaki, H., Tsukita, S., and Furuse, M. (2004). JACOP, a novel plaque protein localizing at the apical junctional complex with sequence similarity to cingulin. J. Biol. Chem. *279*, 46014–46022.

Pfeffer, S. R., and Aivazian, D. (2004). Targeting Rab GTPases to distinct membrane compartments. Nat. Rev. Mol. Cell Biol. *5*, 886–896.

Sahlender, D. A., Roberts, R. C., Arden, S. D., Spudich, G., Taylor, M. J., Luzio, J. P., Kendrick-Jones, J., and Buss, F. (2005). Optineurin links myosin VI to the Golgi complex and is involved in Golgi organization and exocytosis. J. Cell Biol. *169*, 285–295.

Saitou, M., Fujimoto, K., Doi, Y., Itoh, M., Fujimoto, T., Furuse, M., Takano, H., Noda, T., and Tsukita, S. (1998). Occludin-deficient embryonic stem cells can differentiate into polarized epithelial cells bearing tight junctions. J. Cell Biol. *141*, 397–408.

Saitou, M., Furuse, M., Sasaki, H., Schulzke, J. D., Fromm, M., Takano, H., Noda, T., and Tsukita, S. (2000). Complex phenotype of mice lacking occludin, a component of tight junction strands. Mol. Biol. Cell *11*, 4131–4142.

Schneeberger, E. E., and Lynch, R. D. (2004). The tight junction: a multifunctional complex. Am. J. Physiol. *286*, C1213–C1228.

Schock, F., and Perrimon, N. (2002). Molecular mechanisms of epithelial morphogenesis. Annu. Rev. Cell Dev. Biol. *18*, 463–493.

Seabra, M. C., and Wasmeier, C. (2004). Controlling the location and activation of Rab GTPases. Curr. Opin. Cell Biol. *16*, 451–457.

Shen, L., and Turner, J. R. (2005). Actin depolymerization disrupts tight junctions via caveolae-mediated endocytosis. Mol. Biol. Cell *16*, 3919–3936.

Stevenson, B. R., and Begg, D. A. (1994). Concentration-dependent effects of cytochalasin D on tight junctions and actin filaments in MDCK epithelial cells. J. Cell Sci. *107*, 367–375.

Strom, M., Hume, A. N., Tarafder, A. K., Barkagianni, E., and Seabra, M. C. (2002). A family of Rab27-binding proteins. Melanophilin links Rab27a and myosin Va function in melanosome transport. J. Biol. Chem. *277*, 25423–25430.

Suzuki, T., Nakamoto, T., Ogawa, S., Seo, S., Matsumura, T., Tachibana, K., Morimoto, C., and Hirai, H. (2002). MICAL, a novel CasL interacting molecule, associates with vimentin. J. Biol. Chem. *277*, 14933–14941.

Takai, Y., Sasaki, T., and Matozaki, T. (2001). Small GTP-binding proteins. Physiol. Rev. *81*, 153–208.

Terman, J. R., Mao, T., Pasterkamp, R. J., Yu, H. H., and Kolodkin, A. L. (2002). MICALs, a family of conserved flavoprotein oxidoreductases, function in plexin-mediated axonal repulsion. Cell *109*, 887–900.

Thiery, J. P. (2003). Epithelial-mesenchymal transitions in development and pathologies. Curr. Opin. Cell Biol. *15*, 740–746.

Tsukita, S., Furuse, M., and Itoh, M. (2001). Multifunctional strands in tight junctions. Nat. Rev. Mol. Cell Biol. *2*, 285–293.

Utech, M., Ivanov, A. I., Samarin, S. N., Bruewer, M., Turner, J. R., Mrsny, R. J., Parkos, C. A., and Nusrat, A. (2005). Mechanism of IFN-γ-induced endocytosis of tight junction proteins: myosin II-dependent vacuolarization of the apical plasma membrane. Mol. Biol. Cell *16*, 5040–5052.

Vasioukhin, V., and Fuchs, E. (2001). Actin dynamics and cell-cell adhesion in epithelia. Curr. Opin. Cell Biol. *13*, 76–84.

Weber, E., *et al*. (1994). Expression and polarized targeting of a rab3 isoform in epithelial cells. J. Cell Biol. *125*, 583–594.

Weide, T., Teuber, J., Bayer, M., and Barnekow, A. (2003). MICAL-1 isoforms, novel rab1 interacting proteins. Biochem. Biophys. Res. Commun. *306*, 79–86.

Wittchen, E. S., Haskins, J., and Stevenson, B. R. (1999). Protein interactions at the tight junction. Actin has multiple binding partners, and ZO-1 forms independent complexes with ZO-2 and ZO-3. J. Biol. Chem. *274*, 35179–35185.

Yamamoto, Y., Nishimura, N., Morimoto, S., Kitamura, H., Manabe, S., Kanayama, H., Kagawa, S., and Sasaki, T. (2003). Distinct roles of Rab3B and Rab13 in the polarized transport of apical, basolateral, and tight junctional

membrane proteins to the plasma membrane. Biochem. Biophys. Res. Commun. *308*, 270–275.

Yu, A. S., McCarthy, K. M., Francis, S. A., McCormack, J. M., Lai, J., Rogers, R. A., Lynch, R. D., and Schneeberger, E. E. (2005). Knockdown of occludin expression leads to diverse phenotypic alterations in epithelial cells. Am. J. Physiol. *288*, C1231–C1241.

Zahraoui, A., Joberty, G., Arpin, M., Fontaine, J. J., Hellio, R., Tavitian, A., and Louvard, D. (1994). A small rab GTPase is distributed in cytoplasmic vesicles in non polarized cells but colocalizes with the tight junction marker ZO-1 in polarized epithelial cells. J. Cell Biol. *124*, 101–115.

Zerial, M., and McBride, H. (2001). Rab proteins as membrane organizers. Nat. Rev. Mol. Cell Biol. *2*, 107–117.